Applied Thermal Engineering 274 (2025) 126798

Contents lists available at ScienceDirect

Applied Thermal Engineering

journal homepage: www.elsevier.com/locate/apthermeng

Research Paper

Cycling experiments on redox characteristics of iron-rich coal ash under fluidized bed conditions

Bingjun Du [a,b], Haoyu Tian [c], Yuchen Ma [a], Changhao Ma [a,b], Yang Zhang [a,b,d], Junfu Lyu [a,b,d], Xiwei Ke [b,d,*]

[a] Key Laboratory for Thermal Science and Power Engineering of Ministry Education, Department of Energy and Power Engineering, Tsinghua University, Beijing 100084, China
[b] Shanxi Research Institute of Huairou Laboratory, Taiyuan 030032, China
[c] Department of Chemical and Biological Engineering, The Hong Kong University of Science and Technology, Clear Water Bay, Kowloon, Hong Kong, China
[d] Beijing Huairou Laboratory, Beijing 101499, China

ARTICLE INFO

Keywords:
Oxygen carrier
Iron-rich coal ash
Redox activity
Indonesian lignite ash
Cycling experiment

ABSTRACT

Oxygen carriers can establish reaction paths between fuels and oxidants and have been widely used in chemical looping systems and oxygen carrier aided combustion. Among various oxygen carriers, iron-rich coal ash with abundant reserves and good physical–chemical characteristics are ignored in present studies. This work aims to determine the redox activity of iron-rich Indonesian lignite (IN) ash via a cycling combustion experiment of biogas including H_2, CH_4, and CO in a bubbling fluidized bed reactor at 700℃, 800℃, and 900℃. Two types of Chinese iron-lean coal ash (Jiaocheng and Shuozhou coal ash) and two typical oxygen carriers (steel slag and ilmenite) were also tested for comparison. Results show that IN ash exhibits significant adsorption capacities and conversion rates for combustible gases (>0.028 mol/g and >17%) and oxygen (>0.02 mol/g and ≥68%), which are generally the highest at 800℃ (0.056 mol/g and 35.0% for combustible gases, 0.024 mol/g and 72.5% for oxygen) due to higher reaction activity and a lower degree of sintering and agglomeration. While these indexes are higher than those of iron-lean coal ash and comparable to those of steel slag and ilmenite, IN ash does not considerably promote partial oxidation of methane or carbon deposition, and its composition remains relatively stable through long-term experiments. The excellent redox activity of Indonesian lignite ash is mainly attributed to its high iron content and good pore characteristics. This work reveals the great potential of iron-rich coal ash to be applied as an oxygen carrier in oxygen-carrying processes and relevant industrial systems.

1. Introduction

Oxygen carriers are substances with strong oxygen-carrying capacities and significant redox activities, which can achieve continuous and efficient redox cycles between oxidizing and reducing agents by introducing sub-reactions with lower activation energies [1]. To be specific, generally two successive reactions occur on the surface of the oxygen carrier in a complete redox cycle: the oxygen carrier first adsorbs oxygen atoms from the oxidizing agent (typically gaseous oxygen or steam) and converts them into solid-state lattice oxygen ([O]), then releases the lattice oxygen, oxidizes the reducing agent, and regenerates itself to its pre-adsorption state [1,2].

Oxygen carriers have been widely applied in chemical looping processes, such as chemical looping combustion (CLC), chemical looping gasification (CLG), chemical looping reforming (CLR), chemical looping with oxygen uncoupled (CLOU), and chemical looping hydrogen generation (CLHG) [3–5]. In these scenarios, oxygen carriers can create a high-oxygen, low-nitrogen environment for fuels with low cost, good mass and heat transfer properties, and simple reaction paths, thus improving the reaction kinetics and achieving the enrichment of exhaust gases naturally at the same time, which is highly conducive to cost-effective and low-energy-penalty exhaust treatment and CO_2 capture [2,3,6]. In addition to applications in the field of chemical looping processes, oxygen carriers can also be applied as alternative bed materials in circulating fluidized bed (CFB) boilers to achieve a more even oxygen and temperature distribution and higher combustion efficiency, which is called oxygen carrier aided combustion (OCAC) [3,7]. Thunman et al. [3] first proposed and practiced this concept by using ilmenite

* Corresponding author at: Shanxi Research Institute of Huairou Laboratory, Taiyuan 030032, China.
E-mail address: kexiwei@sxri.hrl.ac.cn (X. Ke).

https://doi.org/10.1016/j.applthermaleng.2025.126798
Received 12 February 2025; Received in revised form 30 April 2025; Accepted 10 May 2025
Available online 11 May 2025

as bed material in a 12 MW_{th} biomass-fired CFB boiler. They found that ilmenite addition improved oxygen distribution in the furnace and inhibited CO and NO emissions compared with operation with only silica sand.

Scholars have been exploring the characteristics and performance of various metal ores or synthetic metal oxides including Mn, Fe, Co, Ni, Cu, and other elements as oxygen carriers [2,8–12]. Among these substances, iron-based oxygen carriers have attracted extensive attention and have been widely used in chemical looping applications [2]. Typical iron-based oxygen carriers have the advantages of abundant reserves, low cost, environmental compatibility, and high mechanical strength [6]. Moreover, iron has multiple valences and oxidation states (including Fe_2O_3, Fe_3O_4, FeO, and Fe), indicating high redox activities [13].

Raw iron-containing ores, including hematite and ilmenite [6,14–18], are naturally good oxygen carriers for their considerable redox activities and affordable prices. Barros do Nascimento [15] tested three iron ores from Brazil with low cost and abundance in nature, and found the activation process of their redox activities during redox cycles. Moreover, the reactivity is positively correlated with the content of the Fe_2O_3 phase. Ma et al. [17] evaluated the performance of the hematite ore in the OCAC by using the Chifeng lignite as the solid fuel in a batch fluidized bed reactor. They found that higher CO_2 generation and low NO conversion were simultaneously achieved, and the impact of the pulsed batches of coal was inhibited (which they called the "peak load shifting" effect), along with minimal surface changes of the used OC. Schneider et al. [18] examined the oxygen distribution profiles and their shift by low-cost ilmenite during methane combustion. Results showed the shift trend of oxygen from the lower part of the reactor to the reduction-dominated zone with the help of ilmenite compared with silica sand, which resulted in many positive effects including CO_2 increase from combustion enhancement. While the main issues faced by simple iron-based oxygen carriers are relatively lower reactivities due to high activation energy and equilibrium limitation of the chemical reactions, and potential sintering, agglomeration, and carbon deposition problems [2,5,19], various synthetic iron-based catalysts, prepared by different methods with different supports and co-catalysts, usually exhibit higher redox activity and strong stability, but often bring high material and economy cost [5,6].

Some industrial iron-containing wastes can also be utilized as excellent oxygen carriers to achieve low-cost approaches for solid waste recycling [2,7,20]. Rydén et al. [7] proposed the utilization of Linz-Donawitz (LD)-slag, which is the second largest by-product in the steel making process, as an active bed material in a 12 MW_{th} CFB boiler using wood chips as fuel. During the experiments, fuel conversion in the boiler was promoted, and severe agglomeration or sintering of the bed material was not detected. However, the addition of LD-slag brought some other problems such as high fly ash, CO, and NO concentrations in the flue gas. Ksepko [20] prepared sewage sludge ash with rich Fe_2O_3 content and tested its redox activity via cyclic redox experiments in a thermogravimetric (TG) analyzer. Results showed that the sewage sludge ash can react with hydrogen and coal with a remarkable reaction rate at around 750–800℃ (generally lower than pure Fe_2O_3-based oxygen carrier). Moreover, it also showed high mechanical strength and low agglomeration tendency during the experiments. Besides the wastes mentioned above, one iron-rich solid waste should be paid more attention to—iron-rich coal ash, which shows great potential to be an excellent oxygen carrier for the following reasons:

①Coal ash is one of the industrial solid wastes with a huge amount to be disposed of every year, so its utilization yields environmental benefits;
②Coal ash is significantly cheaper (typically < 40 $/t in China) than iron ores and synthetical catalysts, and its utilization as an oxygen carrier is also significantly cheaper than expensive hazardous solid waste treatment strategy;
③Coal ash naturally has a suitable particle size range (1 μm ~ 500 μm) and a high specific surface area conducive to fluidization, gas adsorption, and gas–solid reactions;
④Coal ash usually has good mechanical and chemical stability, which is crucial to long-term stable operation. When used in reactors, it also has a scouring and cleaning effect on the contaminated layer on the reactors' inner surface;
⑤Good pore characteristics and rich iron content in iron-rich coal ash usually indicate strong oxygen-carrying capacity and high redox activity. Besides, in most cases, iron-rich coal ash is also rich in other mineral elements (such as Mg, Al, and Ca) that can act as co-catalysts in the reaction process and alleviate particle sintering and agglomeration [2,5,6];

These characteristics show the potential industrial use of iron-rich coal ash as an excellent oxygen carrier in the future. However, until now, to the best of the authors' knowledge, while there have been some strategies for recycling and utilization of coal ash, such as producing cement [21], fire resistance blocks [22], and ceramic tiles [23], no practical use has been found yet for iron-rich coal ash as an oxygen carrier, and its practical oxygen-carrying performance and redox activity remain to be further studied.

This study takes Indonesian lignite (IN) ash as an example of iron-rich coal ash and determines its oxygen-carrying capacity and redox activity via a combustion process of combustible gases including H_2, CH_4, and CO. IN along with other coal ash and typical oxygen carriers was characterized using a Malvern laser particle size analyzer, X-ray diffraction (XRD) and X-ray fluorescence (XRF) analysis, and nitrogen adsorption test before the experiment. Redox cycling experiments were conducted on a bubbling fluidized bed reactor under various temperatures, yielding a qualitative and quantitative description of the redox performance of the iron-rich coal ash under various conditions.

2. Material and methods

2.1. Sample preparation and characterization

2.1.1. Sample preparation

This research used Indonesian lignite ash as the test sample. Indonesia is the world's largest exporter of coal (by weight), with total exports of 521 Mt, and more than 85% of the total Indonesian coal exported is lignite or sub-bituminous coal [24,25]. Indonesian lignite is extensively consumed around the world and thus produces large amounts of iron-rich lignite ash due to its rich iron content (Around 11.5 Mt/a, estimated from the data above and the ash content in IN tested in this paper, See Table S1 in the Supplementary Material for the proximate analysis of IN). For comparison, this research also used two kinds of typical iron-lean Chinese bituminous coal ash: Jiaocheng coal ash (JC ash) and Shuozhou coal ash (SZ ash), and two typical oxygen carriers: steel slag (SS) and ilmenite (IL).

Before the experiment, the Indonesian lignite was crushed into particles of about 1 cm. The lignite particles were then laid on an iron tray with a thickness of about 2 cm and fed into a Muffle furnace for combustion in the air at 850℃. After 6 h of combustion, the lignite ash generated was then sieved for more than 3 h. The preparation processes of JC ash and SZ ash from Jiaocheng coal and Shuozhou coal were the same as above (See Table S1 and Table S2 in the Supplementary Material for the proximate analysis and ultimate analysis of Indonesian lignite, Jiaocheng coal, and Shuozhou coal). Ilmenite was directly sieved for 1 h, and steel slag was first crushed into particles of around 100 μm and then sieved for 1 h. After these preparation processes for the five materials, particles with a size range of 150 ~ 180 μm were sieved and used for experiments. This size range is consistent with the normal size range of bed material flowing inside the CFB reactor. The analysis result of the Malvern laser particle size analyzer showed that the Dv (50) of the sieved IN ash is 210 μm, which met the expectation and could be used for

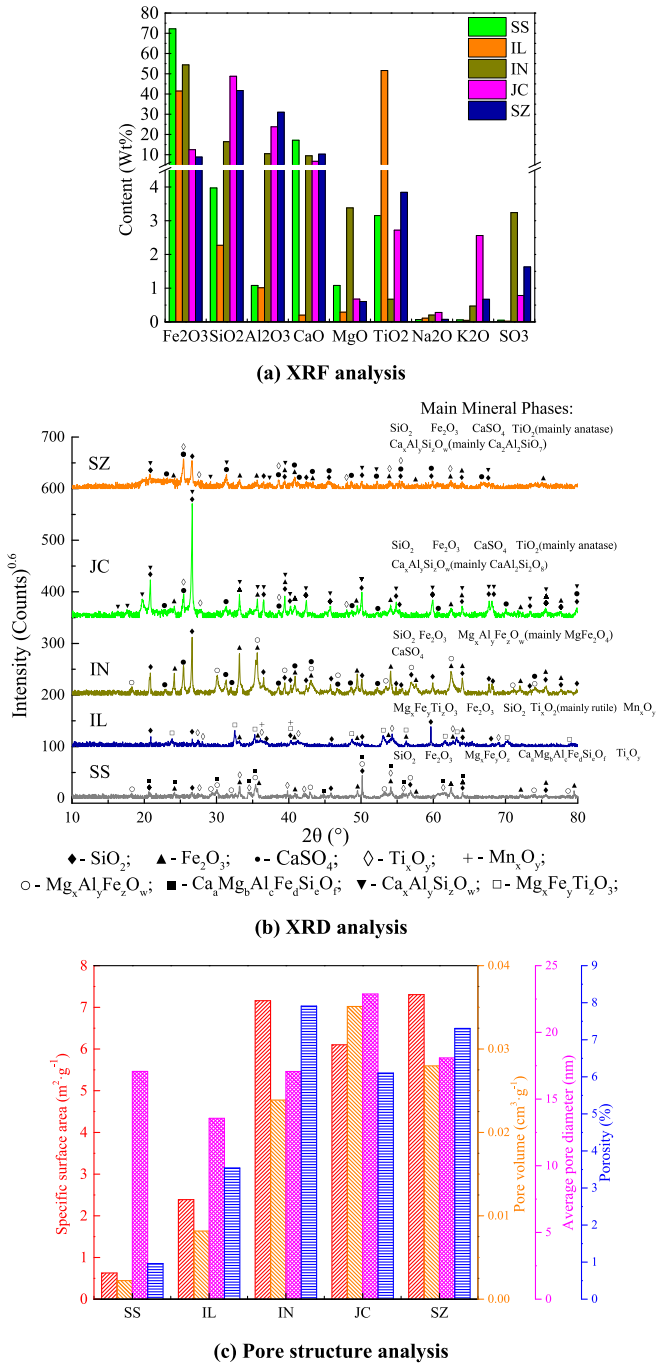

Fig. 1. Characterization results of different material samples used in the experiments.

the following experiments.

2.1.2. Composition analysis

The compositions of all five materials were analyzed via XRD and XRF methods. The analysis results of XRF for all five materials are shown in Fig. 1(a) (See Table S3 in Supplementary Material for detailed data). In terms of mass fraction, the order of main metal element contents (in oxide forms) of IN ash by weight from high to low is Fe (54.4%), Si (16.40%), Al (10.45%), Ca (9.44%), and Mg (3.38%). Compared with JC ash and SZ ash, IN ash has significantly higher Fe content (which is even higher than ilmenite, but lower than steel slag) and the highest Mg content (3.38%) and S content (3.24%), proving that it is iron-rich coal ash. The Si and Al contents of IN are between those of typical oxygen carriers and the other two kinds of coal ash. In addition, ilmenite has an extremely higher Ti content (51.59%) than other materials, steel slag has the highest Ca content (17.15%), and SZ ash has significantly higher K content (2.56%) than other materials.

The XRD patterns for all materials are shown in Fig. 1(b). The main mineral phases of the three kinds of coal ash (IN, JC, and SZ ash) are similar (that is, Fe_2O_3, SiO_2, $CaSO_4$, and composite oxide of Mg, Al, and Fe, mainly $MgFe_2O_4$). Because the Fe content of steel slag and the Ti content of ilmenite are higher, more compounds are formed among Fe (or Ti) and other elements for these two materials.

2.1.3. Pore structure analysis

Through the nitrogen adsorption test (using the Brunauer-Emmett-Teller Method), the pore structure analysis results of all materials are shown in Fig. 1(c). Compared with the iron-rich ilmenite and steel slag, IN ash has the highest porosity and larger specific surface area and pore volume, resulting in a positive impact on gas adsorption and gas–solid reactions.

2.2. Experimental system

The experiment determines the oxygen-carrying capacity and redox activity via a combustion process between combustible gases and oxygen, referring to the redox process between oxygen carriers and biomass in real industrial processes. The diagram of the entire experimental system is shown in Fig. 2. In previous studies, oxygen carriers participate in biomass combustion mainly through gas–solid reactions with combustible volatile gas rather than directly affecting biomass pyrolysis and char conversion processes. In addition, most agricultural and forestry biomass has high volatile content and low char content. Therefore, main combustible volatile components are applied as model fuels for biomass and the combustible gas used in this experiment, which consists of 26% H_2, 38% CH_4, and 36% CO referring to the pyrolysis products of straw [4,12,15]. The oxidizing gas, referring to air, is obtained by mixing the gas from O_2 and Ar gas cylinders with a volume ratio of 21:79.

The reaction process occurs in a customized vertical quartz tube with a height of 1209 mm and an inner diameter of 40 mm. A quartz sintered plate gas distributor is installed in the tube 580 mm in height from the bottom for carrying and fluidizing the bed material particles. The tube is externally heated by an electric vertical furnace and equipped with a differential manometer and K-type thermocouples for bed pressure drop and bed temperature measurement.

The inlet gases first flow through the mass flowmeters (Qixing Huachuang D07-19B), which are connected to an external automatic controller to achieve precise real-time control of flow rates. Gases are fed into the quartz tube from the bottom pipe and sent to 3 cm below the air distributor after preheating, then fluidize the material particles on the air distributor, and undergo the reaction process. The exhaust gases are filtered and condensed to remove fine particles and steam after exiting the quartz tube through the top pipe, and are finally fed into the online mass spectrometer (TILON SRD200M) for continuous and quantitative gas concentration analysis.

2.3. Experiment procedure

Before the experiment begins, the mass flowmeters and signals of H_2, CH_4, CO, and O_2 in the online mass spectrometer are calibrated. The gas types detected by the mass spectrometer in this experiment and correlated molecular masses are H_2-2, CH_4-15, CO-28, O_2-32, Ar-40, and CO_2-44.

First, 14 g of one material (about 3 cm height on the air distributor for IN ash) is added into the quartz tube on the air distributor. The preset experiment temperatures are 700℃, 800℃, and 900℃, respectively, which refer to most working conditions for typical chemical looping processes and OCAC in CFB boilers. After setting the temperature of the

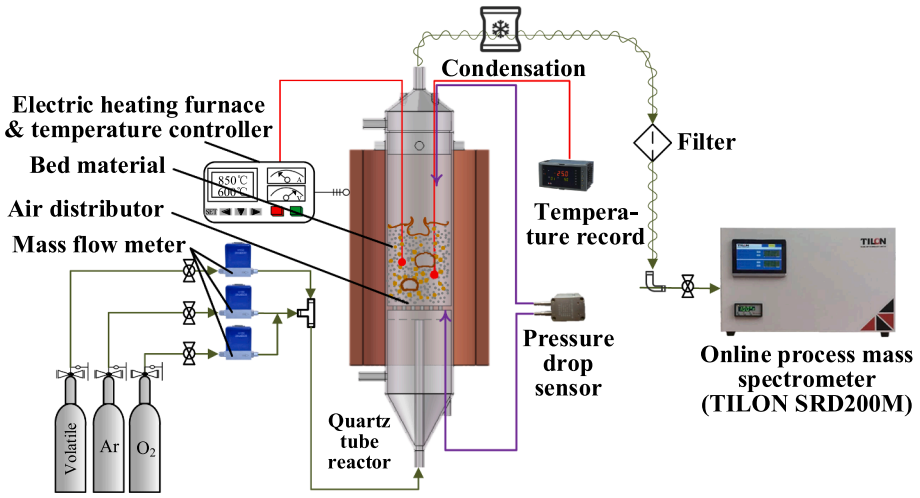

Fig. 2. Experimental system diagram.

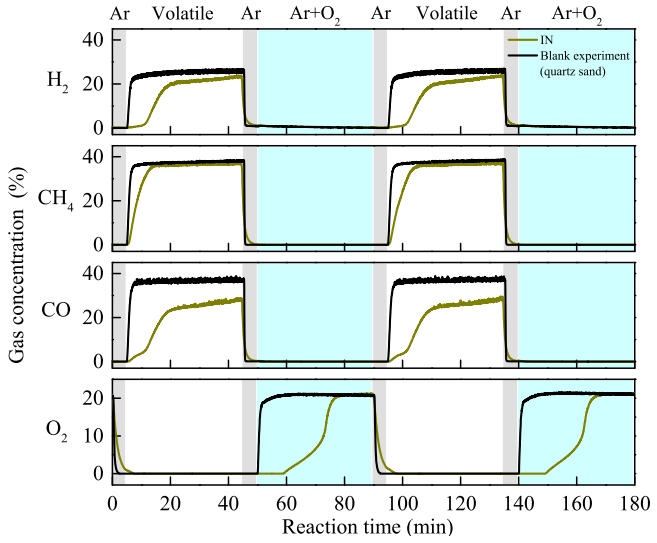

(a) IN ash group and the blank group at 800°C

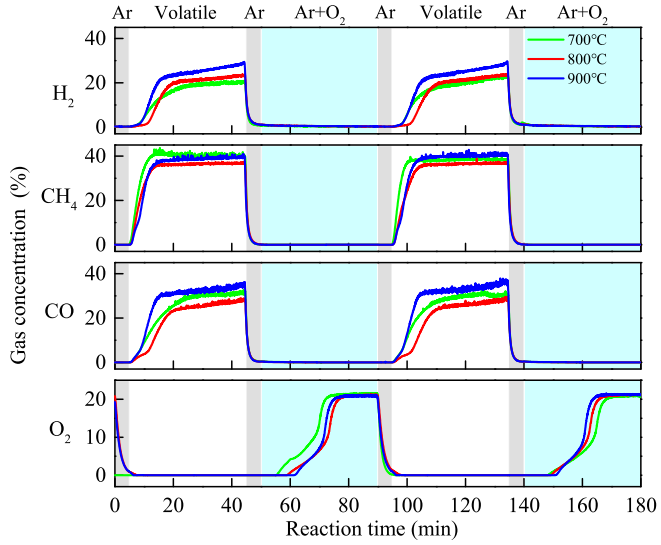

(b) IN ash group under different temperatures

Fig. 3. Gas concentrations as a function of time for the IN ash group.

furnace and opening the mass spectrometer, a stream of Ar with a flow rate of 0.5 L/min is fed into the tube to purge the gas path. When the temperature in the quartz tube reaches the preset value, start gas feeding in the order of "Ar (5 min) – combustible gas (40 min) – Ar (5 min) – oxidizing gas (40 min)" cyclically. Note that in order to save experiment costs, in some cases, the input gas type is immediately switched after the gas concentrations are basically stable during the experiment. The total gas flow rate is controlled to ensure the gas velocity in the quartz tube (0.08 m/s) is slightly larger than the minimum fluidization velocity (around 0.07 m/s) and constant under different temperature conditions.

After 3 cycles (or 30 cycles for long-term experiments), switch the inlet gas and the temperature of the furnace, and then repeat the cycling experiment procedure above. After the cycling experiment for one material is finished, close the furnace, keep the Ar flow with a flow rate of 0.5 L/min to cool the tube and samples, and switch the type of the material after the tube is cooled to room temperature. After the entire set of cycling experiments is finished, the signal intensity data of the mass spectrometer are saved for subsequent data processing.

3. Results and discussion

3.1. Redox activity of IN ash

Fig. 3(a) shows gas concentrations as a function of time in two cycles for both the IN ash group and the blank group at 800°C. Compared with the blank group, under the influence of IN ash, concentrations of all gases at the same reaction time and the climbing rates of gas concentrations significantly decrease, and the required time for gas concentrations to reach stability is significantly extended. While oxygen concentration for the blank group quickly reached 21% right after oxygen injection, it took 5 ~ 10 min for the mass spectrometer to detect any positive signal intensity of oxygen (while it takes around 1 min for gases to flow from the mass flowmeter to the mass spectrometer) and around 30 min to detect 21% oxygen concentration after oxygen injection.

These phenomena indicate that IN ash has a large gas adsorption capacity and strong redox activity, namely, significant heterogeneous redox reactions can occur on the IN ash surface, including elementary reactions of reducing gases with active oxygen atoms:

$$CH_4 + 4O^* \rightarrow CO_2 + 2H_2O \quad (1)$$

$$H_2 + O^* \rightarrow H_2O \quad (2)$$

$$CO + O^* \rightarrow CO_2 \quad (3)$$

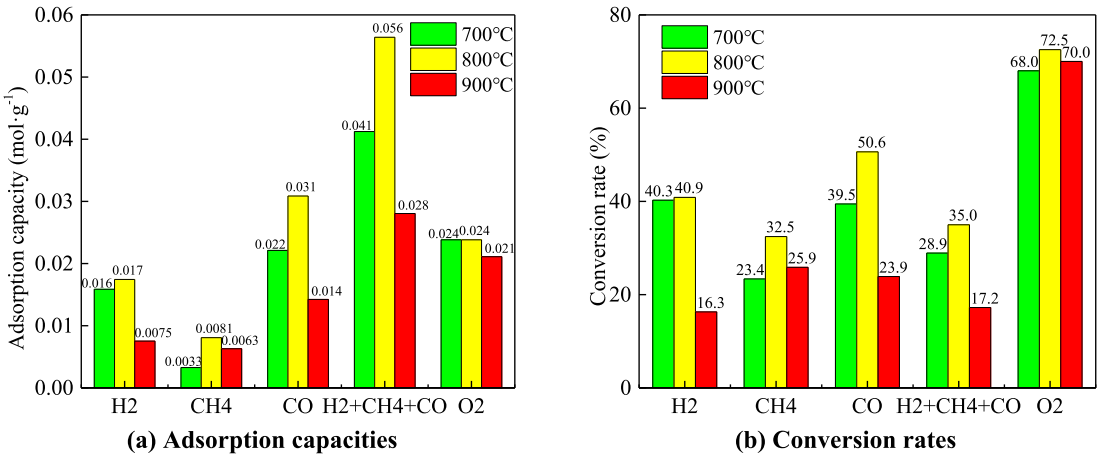

Fig. 4. Quantitative indexes of IN ash for different gases.

And the reaction of oxygen dissociation to regenerate active oxygen atoms:

$$O_2 + 2(*) \rightarrow 2O* \tag{4}$$

Under different temperatures, gas concentrations as a function of time in two cycles for the IN ash group are shown in Fig. 3(b). Temperature has an insignificant impact on the global reaction process. After combustible gas injection, gas concentrations first increase, then remain stable or, for some working conditions and some gaseous species (such as CO concentration), still increase slowly and do not reach the equilibrium gas concentration of the blank experiment at the end of the ventilation time. Therefore, the reaction process can be roughly split into two stages: combustible gases first participate in gas–solid reactions on the surface of IN ash, after the lattice oxygen on the particle surface is depleted, they diffuse into IN ash particles to react with the lattice oxygen in the particle. While the first stage is usually fast, the second stage is always significantly slower considering the strong mass transfer resistance within the particle [26,27].

In order to further analyze the redox activity of IN ash and other materials, the following indexes are introduced for quantitative description.

(1) Adsorption capacity. This index symbolizes the excess gas adsorption on the material particle surface compared with the blank experiment (in which there is also a small amount of gas adsorbed on the surface of silica sand), which describes how much molar quantities of one gas participate in heterogeneous reactions with the material particles or is physically adsorbed on material particle surfaces, and indicates the redox activity of the material particle with the gas. The adsorption capacity of material Y for gas X per gram is defined as:

$$C_{X,Y} = \left[\sum_{t_{j,0}=t_i}^{t_s} c_{X,0}(t_{j,0}) \dot{Q}_{\text{out},0}(t_{j,0}) \Delta t_{j,0} - \sum_{t_{j,Y}=t_i}^{t_s} c_{X,Y}(t_{j,Y}) \dot{Q}_{\text{out},Y}(t_{j,Y}) \Delta t_{j,Y} \right] / m_Y \tag{5}$$

where the subscript X represents the gas type, Y represents the material type, and 0 represents the blank group. m_Y is the mass of the material (equal to 14 g for all materials). $c_{X,0}$ and $c_{X,Y}$ are the concentrations of gas X in the tube (unit mol/m^3) for the blank group and the material Y group, respectively. t_i is the time when the concentration of gas X in the blank experiment begins to increase, and t_s is the time when the concentration of gas X in the experiment for material Y increases to 95% of the maximum concentration in one gas-feeding cycle. Δt_j is the time interval between t_j and t_{j+1} corresponding to the sampling interval of the mass spectrometer (unit s for all the time above).

$\dot{Q}_{\text{out}}$ is the total outlet gas volume flow rate. During experiments, while the total inlet gas volume flow rate $\dot{Q}_{\text{in}}$ is kept constant (equal to 0.1 L/s for all materials under all temperatures) during experiments, $\dot{Q}_{\text{out}}$ is not constant because not all reactions during experiments are constant volume reactions (such as Eq. (1) and Eq. (4), water vapor is not condensed in the tube). Therefore, if ignoring side reactions and excess physical adsorption of gases compared with the blank experiment on material particle surfaces, and supposing all gases obey the ideal gas equation, then:

$$\dot{Q}_{\text{out},0} = \dot{Q}_{\text{in}} \cdot \frac{1 - c_{X,\text{in}}}{1 - c_{X,0}} \tag{6}$$

$$\dot{Q}_{\text{out},Y} = \dot{Q}_{\text{in}} \cdot \frac{1 - c_{X,\text{in}}}{1 - c_{X,Y}} \tag{7}$$

where $c_{X,\text{in}}$ represents the concentration of gas X before entering the quartz tube (that is, the initial concentration of gas X in the gas cylinder), X represents CH_4 during volatile injection (initial CO + H_2 and CO_2 + H_2O they generated as the internal standard), and O_2 during oxygen injection (Ar as the internal standard).

The adsorption capacities of IN ash for H_2, CH_4, CO, and O_2 in the experiment can be calculated using the data shown in Fig. 3(b) based on Eq. (5) ~ Eq. (7) (the results are averaged over the calculated values from the two cycles, the same hereinafter), as shown in Fig. 4(a). Moreover, the adsorption capacity of IN ash for the combustible gas mixture can be calculated as:

$$C_{\text{Conbustible gas},Y} = C_{\text{H}_2,Y} + C_{\text{CH}_4,Y} + C_{\text{CO},Y} \tag{8}$$

Interestingly, the highest adsorption capacity of IN ash does not occur under the highest temperature condition. Instead, at 800°C, the adsorption capacity is the highest (0.17 mol/g, 0.0081 mol/g, 0.0316 mol/g, 0.056 mol/g, and 0.024 mol/g for H_2, CH_4, CO, combustible gas, and O_2, respectively). Among combustible gases, the adsorption capacity of IN ash for CO is the highest and CH_4 the lowest, which indicates that in the preset combustible gas atmosphere, CO adsorption and reactions are dominant,

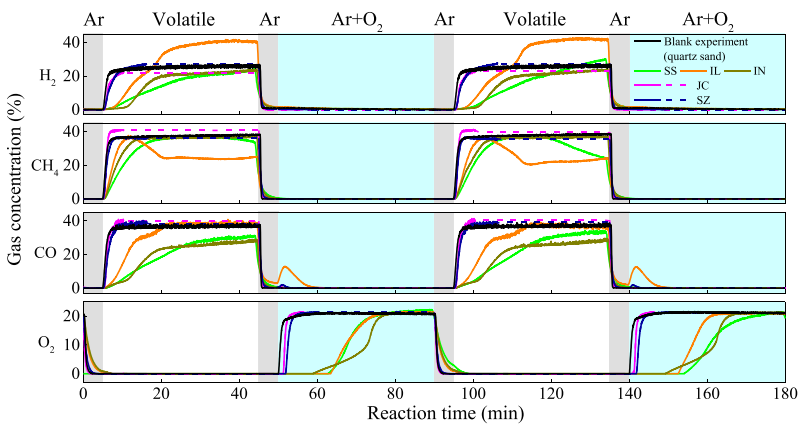

(a) All groups at 800℃

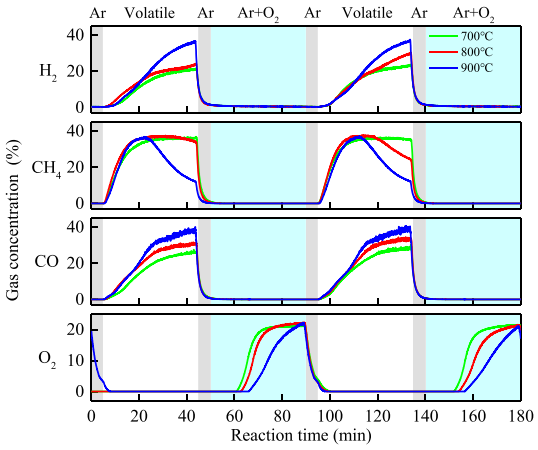

(b) Steel slag group under different temperatures

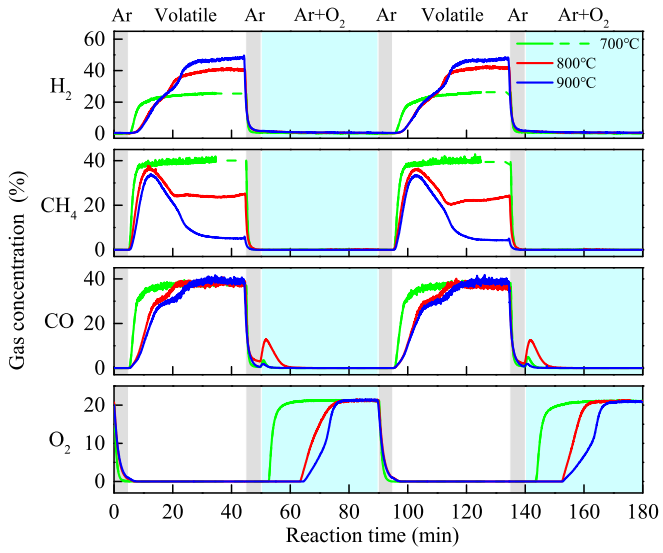

(c) Ilmenite group under different temperatures

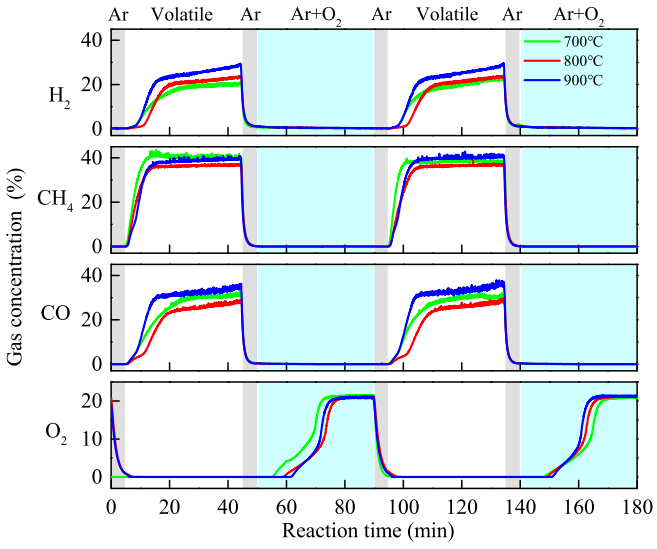

(d) IN ash group under different temperatures

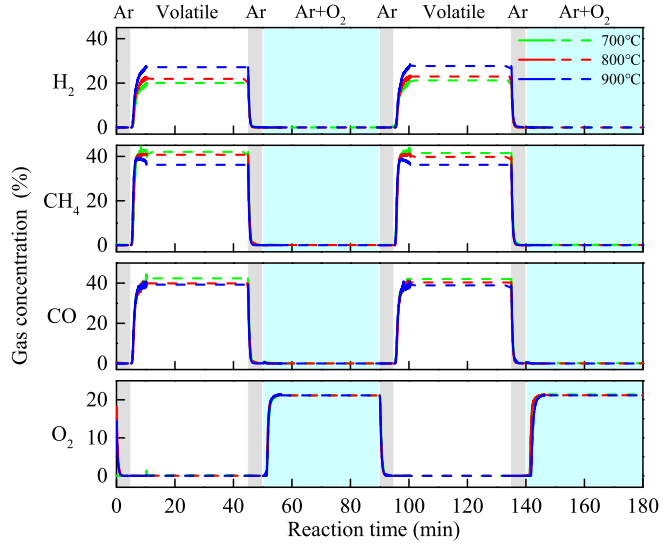

(e) JC ash group under different temperatures

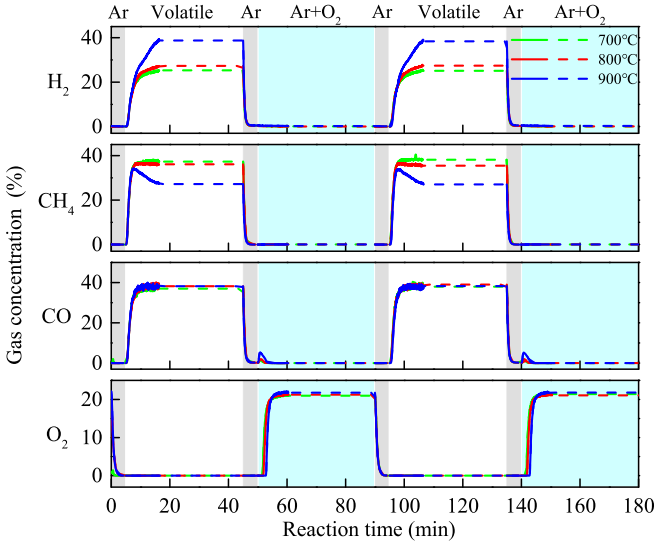

(f) SZ ash group under different temperatures

Fig. 5. Gas concentrations as a function of time for different material groups under different temperatures Note: the dashed lines indicate that the input gas types were switched after the concentrations were basically stable during the experiment, and the concentrations of these gases can be regarded as unchanged in this time range. The meaning is the same for Fig. 6.

(2) Conversion rate. This index is calculated by dividing the total output molar quantities of the gas in the blank experiment into the "Adsorption capacity", so it implies the conversion ability and conversion speed of the material for the gas to some extent. The conversion rate of gas X for the case applying material Y is defined as:

$$\alpha_{X,Y}=\frac{\sum_{t_{j,0}=t_i}^{t_s} c_{X,0}(t_{j,0})\dot{Q}_{\mathrm{out},0}(t_{j,0})\Delta t_{j,0}-\sum_{t_{j,Y}=t_i}^{t_s} c_{X,Y}(t_{j,Y})\dot{Q}_{\mathrm{out},Y}(t_{j,Y})\Delta t_{j,Y}}{\sum_{t_{j,0}=t_i}^{t_s} c_{X,0}(t_{j,0})\dot{Q}_{\mathrm{out},0}(t_{j,0})\Delta t_{j,0}} \quad (9)$$

For the case of IN ash, the conversion rates of H_2, CH_4, CO, and O_2 can be calculated using the data shown in Fig. 3(b) based on Eq. (6), Eq. (7), and Eq. (9), as shown in Fig. 4(b). Moreover, the conversion rate of the combustible gas mixture can be calculated as:

$$\alpha_{\mathrm{Combustible\ gas},Y}=\frac{C_{\mathrm{H_2},Y}+C_{\mathrm{CH_4},Y}+C_{\mathrm{CO},Y}}{\sum_{\mathrm{H_2,CH_4,CO}}\left(\sum_{t_{j,0}=t_i}^{t_s} c_{X,0}(t_{j,0})\dot{Q}_{\mathrm{out},0}(t_{j,0})\Delta t_{j,0}\right)} \quad (10)$$

High O_2 conversion rates for the IN ash (>68%) demonstrate its potential to be a good oxygen carrier. Similar to the results of adsorption capacity, at 800℃, the conversion rates of most gases for IN ash are the highest (40.9%, 32.5%, 50.6%, 35.0%, and 72.5% for H_2, CH_4, CO (still the highest among combustible gases), combustible gas, and O_2, respectively).

3.2. Comparison between different materials

Fig. 5(a) compares the gas concentrations as a function of time in two cycles for the five material groups at 800℃. For iron-lean materials (such as JC ash and SZ ash), gas concentrations quickly reach stability after gas injection and have no significant difference from the blank experiment, which indicates poor redox activities. However, gas concentration curves of IN ash are significantly different from the two kinds of coal ash and more similar to those of steel slag and ilmenite, indicating that the redox activity of IN ash can be comparable to these typical efficient oxygen carriers.

Fig. 5(b)~(f) summarize the gas concentrations as a function of time in two cycles for the five material groups under different temperatures. For iron-lean JC ash and SZ ash, similar to the blank group, the temperature has no significant effect on the oxygen concentration curve, indicating low oxygen-related reactivity.

It should be noted that for some materials, at the same reaction time during the injection of combustible gas, as the temperature increases, CH_4 concentration generally decreases while H_2 concentration generally increases (for instance, the SZ ash at 900℃). For iron-rich steel slag and ilmenite, this phenomenon becomes more significant. In addition, at 800℃ and 900℃, during the injection of combustible gas, CH_4 concentrations for steel slag and ilmenite groups first increase, then significantly decrease over time, while H_2 and CO concentrations first increase rapidly, then keep increasing slowly. Particularly, the highest H_2 concentrations for SZ ash, steel slag, and ilmenite groups at 900℃ are remarkably higher (>37%) than the initial H_2 concentration in the gas cylinder (26%). These phenomena indicate that these materials may have certain catalytic effects on the partial oxidation or decomposition of CH_4 (as shown in Eq. (11) and Eq. (12), especially under higher temperatures [28]. However, such catalytic effect may be insignificant for IN ash because CH_4 concentration does not decrease notably as the temperature increases for the IN ash group.

$$CH_4 + O^* \rightarrow CO + 2H_2 \quad (11)$$

$$CH_4 \rightarrow C + 2H_2 \quad (12)$$

It is also worth noting that there is a remarkable increase in CO concentration after oxidizing gas injection for ilmenite, especially at 800℃, which indicates that carbon deposition occurred on its surface during the combustible gas injection period. This is achieved through the methane decomposition reaction (Eq. (12)), or the Boudouard reaction (Eq. (13)) when the lattice oxygen on the surface is insufficient [29]. Subsequently, the deposited carbon can be oxidized into CO (Eq. (14)). Similarly, the SZ ash group shows a slight increase in CO concentration after oxidizing gas injection, especially at 900℃.

$$2CO \rightarrow C + CO_2 \quad (13)$$

$$2C + O_2 \rightarrow 2CO \quad (14)$$

Fig. 6 further provides the recorded CO_2 signal intensity in the reactor outlet under different conditions. During the injection of combustible gas, high CO_2 signal intensities are detected, which mainly come from gas-solid redox reactions between CH_4/CO and lattice oxygen, and generally increase as the temperature increases. For iron-lean JC ash and SZ ash, the CO_2 signal intensities quickly peak and then decrease to nearly zero, indicating that little CO_2 was generated during this period. For the other three iron-rich bed materials, significantly higher CO_2 signal intensities are detected, which roughly experience an evolutionary process of first peaking, then rapidly declining, and then slowly declining. Among the three bed materials, IN ash and steel slag groups have higher CO_2 signal intensities than ilmenite.

During oxygen injection, lower but non-negligible CO_2 signal intensity peaks are detected for some experimental conditions. The SZ ash group shows CO_2 signal intensity peaks under all temperatures, along with its CO concentration peaks (Fig. 5(f)), indicating serious carbon deposition on the SZ ash surface, similar to literature findings [29]. Moreover, two CO_2 concentration peaks are detected for ilmenite at 800℃, in which case CO_2 may originate from the oxidation of residual combustible gas and deposited carbon on the ilmenite surface (Fig. 5(c)). In contrast, the CO_2 signal intensity peaks of the IN ash group are much lower than these two groups. Therefore, the carbon deposition on the surface of IN ash during the cycling redox experiment is negligible.

Following the method introduced in Section 3.1, the adsorption capacities and conversion rates for all five materials under different temperatures are calculated using the data shown in Fig. 5(b)~5(f). The results are summarized in Fig. 7. Note that negative values in graphs indicate that less gas was absorbed during the experiment compared with the blank experiment, or that the gas was generated during the experiment. It can be seen that for IN ash, the adsorption capacities and conversion rates are significantly higher than those of iron-lean JC ash and SZ ash. Meanwhile, some of these values can be comparable to or even better than those of steel slag and ilmenite, which further demonstrates that IN ash has great potential to be an excellent oxygen carrier. These indexes are also approximately positively correlated with iron content (Fig. 1(a)), indicating that iron content should be the main source of redox activity of IN ash.

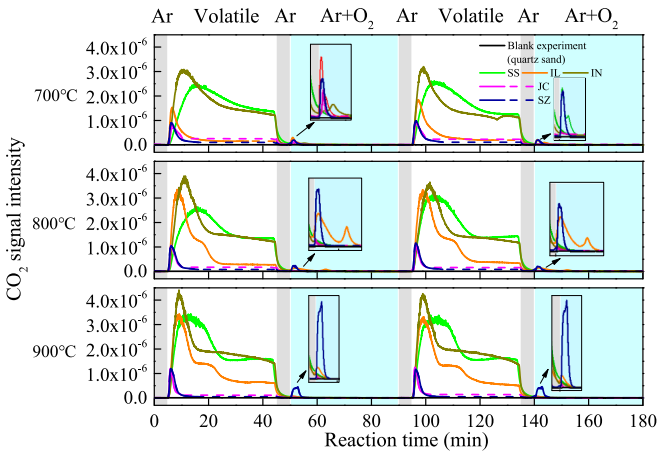

Fig. 6. CO_2 signal intensities as a function of time for different material groups under different temperatures.

3.3. Characteristics of IN ash after long-term experiments

3.3.1. Composition analysis

To evaluate the stability of IN ash during the redox process, long-term redox experiments of IN ash were conducted at 700℃, 800℃, and 900℃, respectively. After 30 redox cycles, the IN ash particles were characterized via XRD, XRF, and pore structure analysis, and compared with the initial IN ash sample.

Fig. 8(a) shows the XRF analysis of IN ash before and after long-term experiments (See Table S4 in Supplementary Material for detailed data). According to the analysis result, after 30 redox cycles, in terms of mass fraction, the main metal element contents of IN ash remain Fe, Si, Al, Ca, and Mg. However, after intensive redox reactions, sulfur content significantly decreased due to sulfate decomposition in a reducing atmosphere. Moreover, considering the physical processes of attrition, sintering, and agglomeration during fluidization, as well as the migration and chemical precipitation of elements during the reaction process, the contents of Si, Al, and Ca detected exhibit certain changes. No significant difference in the mass fraction of other elements was detected.

Fig. 8(b) shows the XRD analysis of IN ash before and after long-term experiments. The main mineral phases of IN ash after long-term experiments are consistent with those of the initial sample (that is, Fe_2O_3, SiO_2, $CaSO_4$, and composite oxide of Mg, Al, and Fe). As the reaction temperature increases, the diffraction peaks of $CaSO_4$ become less significant while the diffraction peaks of aluminosilicate (mainly $CaAl_2Si_2O_8$) become more significant. The former results from the decomposition of $CaSO_4$ in a reducing atmosphere [30], and the latter results from the migration and recombination of the lattice of metal oxides including CaO, Al_2O_3, and SiO_2 during intense cycling redox reactions under high temperature [30,31]. These phenomena are consistent with the XRF analysis results.

Therefore, it can be concluded that the composition of main components with redox activity in IN ash is relatively stable. After long-time operations, its composition changes are within an acceptable range compared with the original IN ash. However, it should be pointed out that even after 30 cycles, the total reaction time is only around 10 h, which is much less than the practical cycling time of typical oxygen carriers in industrial systems. Thus, further industrial-scale studies are still needed.

3.3.2. Pore structure analysis

Through the nitrogen adsorption test (using the Brunauer-Emmett-Teller Method), the pore structure analysis results of IN ash before and after long-term experiments are shown in Fig. 8(c). After long-term experiments, the specific surface area, pore volume, average pore diameter, and porosity of IN ash porosity all decrease with the increase in reaction temperature (except for the average pore diameter at 800℃). While the specific surface area of IN ash experiences a sharp decrease from the condition of 700℃ to 800℃, the pore value and porosity of IN ash experience a sharp decrease from the condition of 800℃ to 900℃. These pore structure changes result from both physical and chemical reasons. Firstly, during the experiments, the fluidization of IN ash leads to frequent and intense collision and friction between ash particles as well as between ash particles and the wall surfaces, which promotes the abrasion and fragmentation of ash particles and lays the foundation for sintering and agglomeration at high temperatures. Secondly, as a result of repeated and strong gas–solid redox reactions, the lattice oxygen content within the ash particles undergoes frequent variation. This promotes the migration of metal elements within the ash particles and the formation of components with low melting points, which, in turn, exerts a notable influence on the pore structure of IN ash under high temperatures [30].

The final redox activity of IN ash is determined by the competition between the intrinsic reaction rate of the active metal components and physical processes during the reaction processes (including adsorption and desorption of gases, and internal and external gas diffusion). On the one hand, the intrinsic redox reaction rates naturally increase as the temperature increases. On the other hand, the specific surface area experiences a significant decrease at high temperatures due to sintering and agglomeration, which has a negative influence on the physical process mentioned above. Therefore, the variation of pore structure and the activity of active components synergistically affect the redox activity of IN ash at different temperatures and thereby determine its optimal reaction temperature (800℃ in this research). However, more research should be conducted using more microscopic characterization methods to reflect the changes in the pore morphology on the particle surface and evaluate the detailed reaction process.

4. Conclusions

As a kind of typical solid waste, iron-rich coal ash can generate considerable economic value when recycled and applied as an oxygen carrier considering its excellent physical and chemical properties. In order to explore the potential and characteristics of iron-rich coal ash as an oxygen carrier, cycling redox experiments were conducted on five different materials including iron-rich Indonesian lignite ash, iron-lean coal ash, and typical oxygen carriers under various temperatures.

Results show that Indonesian lignite ash is an excellent oxygen carrier with high adsorption capacities and conversion rates for H_2, CH_4, CO, and O_2, which are significantly better than iron-lean coal ash and comparable to typical oxygen carriers including steel slag and ilmenite. These characteristics are mainly attributed to the high iron content and good pore characteristics of Indonesian lignite ash. Moreover, no significant partial oxidation of methane and carbon deposition occurred during the experiment, and no significant variation in the composition of active substances was found after long-term experiments. The highest redox activity of Indonesian lignite ash in this research is achieved at 800℃ due to the competitive effect of the reactivity increase and pore structure destruction as the temperature increases.

In the future, more detailed studies about iron-rich coal ash are needed on the microscopic characterization, kinetic parameter

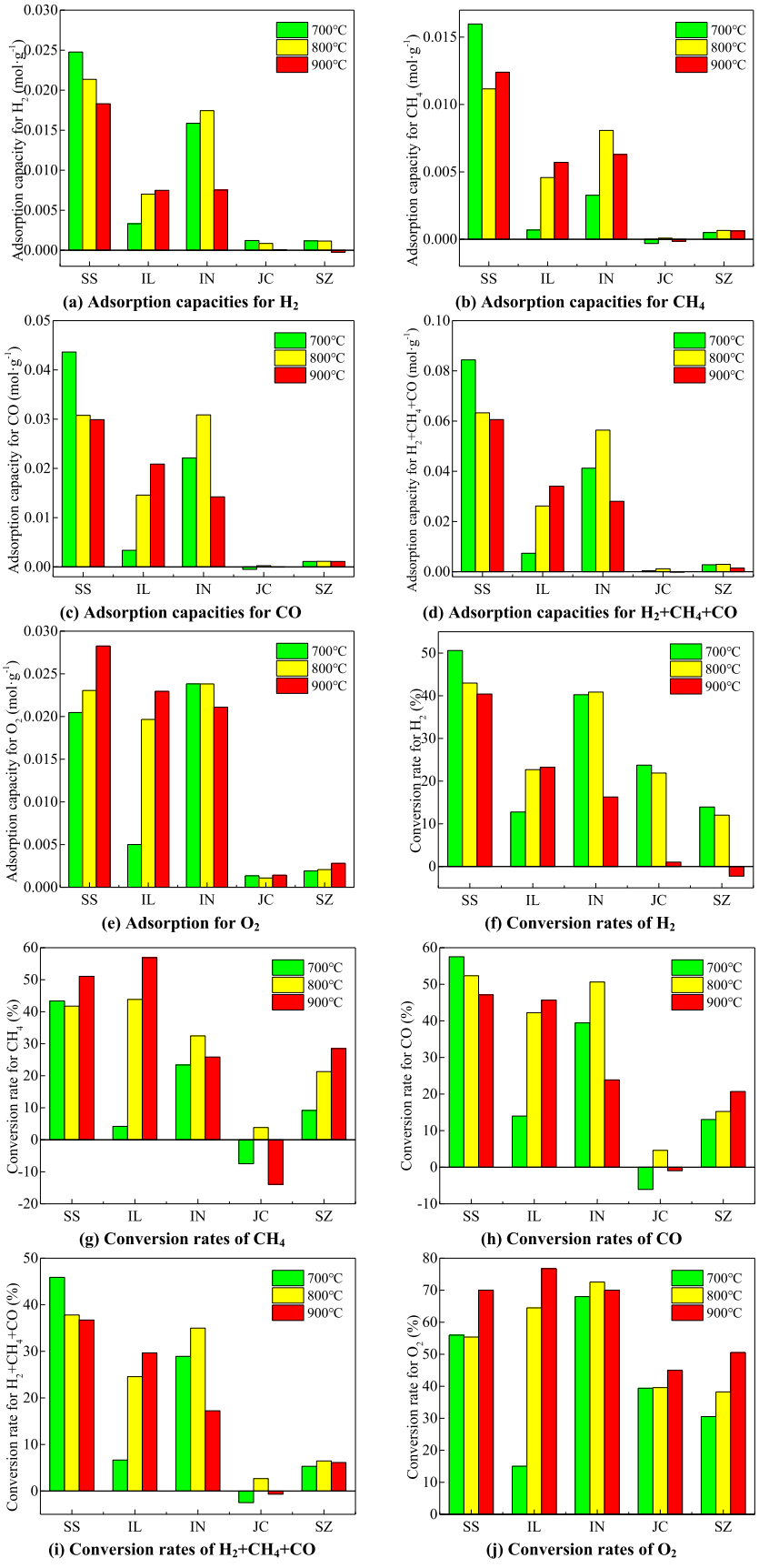

Fig. 7. Summary of quantitative indexes of different materials for different gases.

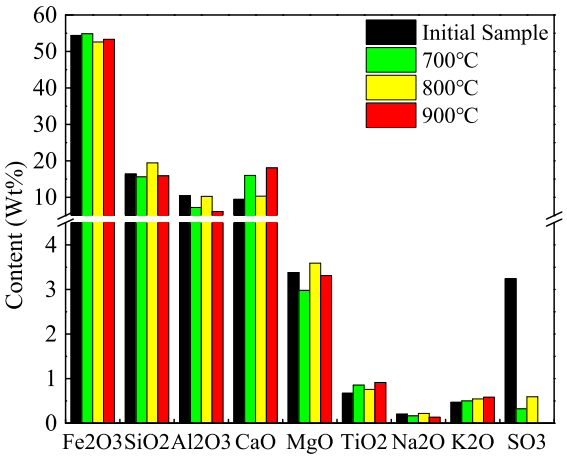

(a) XRF analysis

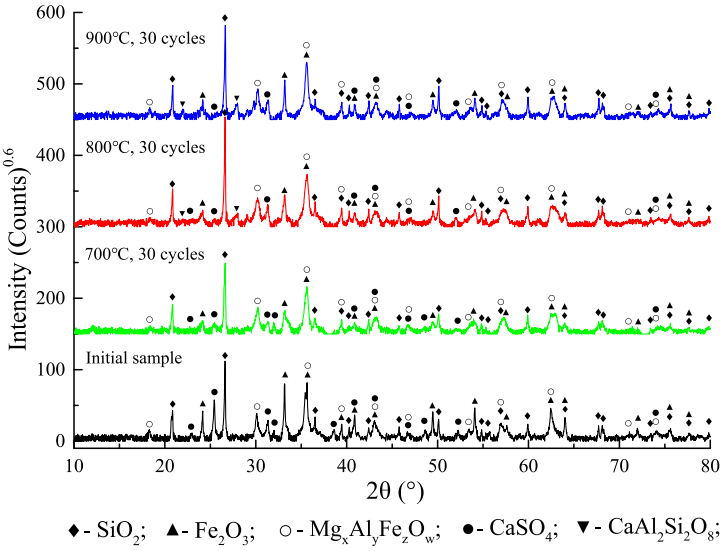

(b) XRD analysis

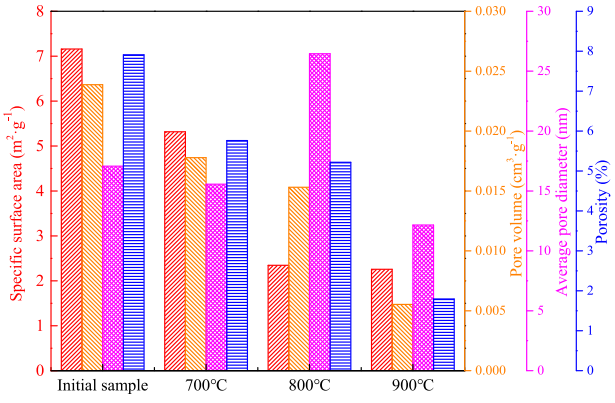

(c) Pore structure analysis

Fig. 8. Characterization results of IN ash before and after long-term experiments.

calculation, and modeling of the detailed reaction mechanism. Moreover, as no similar industrial-scale practice has been conducted until now, the feasibility and economic efficiency of the whole utilization chain need to be further evaluated. (1) From the perspective of practical operations, the operating characteristics in industrial-scale instruments, the effect of flexible composition in iron-rich coal ash, and the stability after long-term operation on the scale of days or even months remain to be explored. (2) From the perspective of the economy, the potential market scale, including the balance between supply and demand also needs further evaluation.

CRediT authorship contribution statement

Bingjun Du: Writing – original draft, Data curation, Formal analysis, Investigation, Methodology, Validation, Visualization. **Haoyu Tian:** Formal analysis, Methodology, Supervision, Conceptualization. **Yuchen Ma:** Writing – original draft, Formal analysis, Methodology, Data curation, Validation, Investigation. **Changhao Ma:** Writing – original draft, Data curation. **Yang Zhang:** Supervision, Conceptualization. **Junfu Lyu:** Supervision, Conceptualization, Resources, Funding acquisition, Project administration. **Xiwei Ke:** Writing – review & editing, Project administration, Methodology, Supervision, Conceptualization, Resources, Funding acquisition.

Declaration of competing interest

The authors declare that they have no known competing financial interests or personal relationships that could have appeared to influence the work reported in this paper.

Acknowledgement

This research was supported by the National Natural Science Foundation of China (No. 52306251); and the Program of Beijing Huairou Laboratory (ZD2023008A).

Appendix A. Supplementary material

Supplementary data to this article can be found online at https://doi.org/10.1016/j.applthermaleng.2025.126798.

Data availability

Data will be made available on request.

References

[1] M. Ishida, D. Zheng, T. Akehata, Evaluation of a chemical-looping-combustion power-generation system by graphic exergy analysis, Energy 12 (1987) 147–154, https://doi.org/10.1016/0360-5442(87)90119-8.
[2] Z. Yu, Y. Yang, S. Yang, Q. Zhang, J. Zhao, Y. Fang, et al., Iron-based oxygen carriers in chemical looping conversions: A review, Carbon. Resour. Convers. 2 (1) (2019) 23–34, https://doi.org/10.1016/j.crcon.2018.11.004.
[3] H. Thunman, F. Lind, C. Breitholtz, N. Berguerand, M. Seemann, Using an oxygen-carrier as bed material for combustion of biomass in a 12-MWth circulating fluidized-bed boiler, Fuel 113 (2013) 300–309, https://doi.org/10.1016/j.fuel.2013.05.073.
[4] G. Liu, G. Lisak, Cu-based oxygen carriers for chemical looping processes: Opportunities and challenges, Fuel 342 (2023) 127828, https://doi.org/10.1016/j.fuel.2023.127828.
[5] Y. Niu, Z. Chi, M. Li, Advancements in biomass gasification research utilizing iron-based oxygen carriers in chemical looping: A review, Mater. Rep.: Energy 4 (3) (2024) 100082, https://doi.org/10.1016/j.matre.2024.100282.
[6] F. Liu, J. Liu, Y. Yang, Research progress and perspectives of solid fuels chemical looping reaction with Fe-based oxygen carriers, Energy Fuel 36 (2022) 9373–9384, https://doi.org/10.1021/acs.energyfuels.2c00961.
[7] M. Rydén, M. Hanning, F. Lind, Oxygen carrier aided combustion (OCAC) of wood chips in a 12 MWth circulating fluidized bed boiler using steel converter slag as bed material, Appl. Sci. 8 (12) (2018) 2657, https://doi.org/10.3390/app8122657.
[8] M. Rydén, M. Hanning, A. Corcoran, F. Lind, Oxygen carrier aided combustion (OCAC) of wood chips in a semi-commercial circulating fluidized bed boiler using manganese ore as bed material, Appl. Sci. 6 (11) (2016) 347, https://doi.org/10.3390/app6110347.
[9] T. Mattisson, M. Johansson, A. Lyngfelt, Multicycle reduction and oxidation of different types of iron oxide particles application to chemical-looping combustion, Energy Fuel 18 (3) (2004) 628–637, https://doi.org/10.1021/ef0301405.
[10] T. Papalas, A.N. Antzaras, A.A. Lemonidou, Unravelling the role of Co in mixed Ni-Co oxygen carriers/catalysts for H2 production via sorption enhanced steam methane reforming coupled with chemical looping, Appl. Catal. B: Env. Energy. 347 (2024) 123777, https://doi.org/10.1016/j.apcatb.2024.123777.
[11] H. Ge, L. Shen, F. Feng, S. Jiang, Experiments on biomass gasification using chemical looping with nickel-based oxygen carrier in a 25 kWth reactor, Appl. Therm. Eng. 85 (2015) 52–60, https://doi.org/10.1016/j.applthermaleng.2015.03.082.
[12] A. Cabello, A. Abad, T. Mendiara, M.T. Izquierdo, L.F. de Diego, Outstanding performance of a Cu-based oxygen carrier impregnated on alumina in chemical looping combustion, Chem. Eng. Journal. 455 (2023) 140484, https://doi.org/10.1016/j.cej.2022.140484.
[13] D. Hu, G. Cao, M. Du, J. Huang, J. Zhao, C. Li, et al., Insight into the biomass pyrolysis volatiles reaction with an iron-based oxygen carrier in a two-stage fixed-bed reactor, Chem. Eng. J. 465 (2023) 142860, https://doi.org/10.1016/j.cej.2023.142860.
[14] C. Jiang, X. Jin, T. Xu, B. Xiao, Z. Hu, X. Wang, Biomass chemical looping gasification for syngas production using modified hematite as oxygen carriers, J. Environ. Sci. 125 (2023) 171–184, https://doi.org/10.1016/j.jes.2021.11.028.
[15] R.A. Barros do Nascimento, H. Pimenta de Macedo, D.M.A. Melo, R.C. Santiago, T. Rodrigues de Araújo, R.L.B.A. Medeiros, et al., Structure and reactivity of Brazilian iron ores as low-cost oxygen carriers for chemical looping combustion, Ind. Eng. Chem. Res. 61 (2022) 2469–2482, https://doi.org/10.1021/acs.iecr.1c03763.
[16] N. Dilmaç, Ö.F. Dilmaç, E. Yardımcı, Utilization of Menteş iron ore as oxygen carrier in Chemical-Looping Combustion, Energy 138 (2017) 785–798, https://doi.org/10.1016/j.energy.2017.07.126.
[17] J. Ma, D. Han, H. Zhao, Investigation on iron ore for the oxygen carrier aided combustion, Fuel Process. Technol. 230 (2022) 107214, https://doi.org/10.1016/j.fuproc.2022.107214.
[18] T. Schneider, J. Krumrein, D. Müller, J. Karl, Investigation of the oxygen supply and distribution in a bubbling fluidized bed by using natural ilmenite for oxygen carrier aided combustion, Energy Fuel 5 (15) (2021) 12352–12366, https://doi.org/10.1021/acs.energyfuels.1c01178.
[19] D. Sanaz, M.H. Sedghkerdar, N. Mahinpey, A review of chemical looping combustion technology: Fundamentals, and development of natural, industrial waste, and synthetic oxygen carriers, Fuel 341 (2023) 127626, https://doi.org/10.1016/j.fuel.2023.127626.
[20] E. Ksepko, Sewage sludge ash as an alternative low-cost oxygen carrier for chemical looping combustion, J. Therm. Anal. Calorim. 116 (2014) 1395–1407, https://doi.org/10.1007/s10973-013-3564-7.
[21] E.R. Teixeira, A. Camões, F.G. Branco, J.B. Aguiar, R. Fangueiro, Recycling of biomass and coal fly ash as cement replacement material and its effect on hydration and carbonation of concrete, Waste Manag. 94 (2019) 39–48, https://doi.org/10.1016/j.wasman.2019.05.044.
[22] C.G. Arenas, M. Marrero, C. Leiva, J. Solís-Guzmán, L.F. Vilches Arenas, High fire resistance in blocks containing coal combustion fly ashes and bottom ash, Waste Manag. 31 (8) (2011) 1783–1789, https://doi.org/10.1016/j.wasman.2011.03.017.
[23] A. Zimmer, C.P. Bergmann, Fly ash of mineral coal as ceramic tiles raw material, Waste Manag. 27 (1) (2007) 59–68, https://doi.org/10.1016/j.wasman.2006.01.009.
[24] International Energy Agency, Coal 2024. https://iea.blob.core.windows.net/assets/a1ee7b75-d555-49b6-b580-17d64ccc8365/Coal2024.pdf; 2024 (accessed 23 January 2025).
[25] International Energy Agency, World Energy Balance 2024. https://www.iea.org/countries/indonesia/coal; 2024 (accessed 23 January 2025).
[26] J. Szekely, J.W. Evans, H.Y. Sohn, Gas-solid Reactions, Academic Press, New York, 1976.
[27] Y. Wang, Z. Li, A DFT-based microkinetic theory for Fe2O3 reduction by CO in chemical looping, Proc. Combust. Inst. 39 (4) (2022) 4447–4455, https://doi.org/10.1016/j.proci.2022.07.026.
[28] D. Yamaguchi, L. Tang, K. Chiang, Pre-oxidation of natural ilmenite for use as an oxygen carrier in the cyclic methane-steam redox process for hydrogen production, Chem. Eng. J. 322 (2017) 632–645, https://doi.org/10.1016/j.cej.2017.04.014.
[29] M. Zhu, S. Chen, S. Ma, W. Xiang, Carbon formation on iron-based oxygen carriers during CH4 reduction period in Chemical Looping Hydrogen Generation process, Chem. Eng. J. 325 (2017) 322–331, https://doi.org/10.1016/j.cej.2017.05.027.
[30] Z. Yang, F. Li, M. Ma, W. Zhao, X. Liu, Y. Wang, et al., Effecting mechanisms of iron-rich sludge on ash fusion characteristics of coal with high ash fusion temperature under reducing atmosphere, Waste Manag. 174 (2024) 328–339, https://doi.org/10.1016/j.wasman.2023.12.011.
[31] L. Xie, Y. Lv, L. Xu, The influence of the high potassium biomass on the ash fusion characteristics of coal, J. Energy Inst. 95 (2021) 52–60, https://doi.org/10.1016/j.joei.2020.12.005.